Available online at www.sciencedirect.com
ScienceDirect
European Journal of Pharmaceutics and Biopharmaceutics 67 (2007) 597–611
European Journal of Pharmaceutics and Biopharmaceutics
www.elsevier.com/locate/ejpb

Research paper

Preparation and characterization of radioactive dirhenium decacarbonyl-loaded PLLA nanoparticles for radionuclide intra-tumoral therapy

Misara Hamoudeh [a], Hani Salim [b], Dumitru Barbos [c], Coustantin Paunoiu [c], Hatem Fessi [a,*]

[a] *Pharmaceutical Technology Department, LAGEP Laboratory Université Claude Bernard (Lyon1) (UCB), Villeurbanne, France*
[b] *Laboratoire de chimie organique-Photochimie et synthèse (Cheops), Université Claude Bernard (Lyon1) (UCB), Villeurbanne, France*
[c] *Institute for Nuclear Research, County: Arges, Romania*

Received 16 February 2007; accepted in revised form 2 April 2007
Available online 14 April 2007

Abstract

This study describes the development of biocompatible radioactive rhenium-loaded nanoparticles for radionuclide anti-cancer therapy. To achieve this goal, dirhenium decacarbonyl [$Re_2(CO)_{10}$] has been encapsulated in poly(L-lactide) based nanoparticles by an oil-in-water emulsion–solvent evaporation method. A 3^3 factorial design method was applied to investigate the influence of both the proceeding and formulation parameters including the stirring speed and the concentration of both the PLLA polymer and the poly(vinyl alcohol) stabiliser on both nanoparticles size and the $Re_2(CO)_{10}$ encapsulation efficacy. The factorial design results attributed a clear negative effect for the stirring speed and the stabiliser concentration on the nanoparticles size while the polymer concentration exhibited a positive one. Regarding the $Re_2(CO)_{10}$ encapsulation efficacy, higher values were obtained when higher polymer concentrations, lower stabiliser concentrations or slower stirring speeds were applied in the preparation. Different tests were thereafter performed to characterize the $Re_2(CO)_{10}$-loaded nanoparticles. The nanoparticles size, being experimentally controlled by the above mentioned parameters, ranged between 330 and 1500 nm and the maximum rhenium loading was 24% by nanoparticles weight as determined by atomic emission assays and neutron activation analysis. Furthermore, the rhenium distribution within nanoparticles has been shown to be homogeneous as confirmed by the energy dispersive X-ray spectrometry. DSC assays demonstrated that $Re_2(CO)_{10}$ was encapsulated in its crystalline initial state. Other experiments including FT-IR and NMR did not show interactions between PLLA and $Re_2(CO)_{10}$. To render them radioactive, these nanoparticles have been bombarded with a neutron flux of 1.45×10^{13} n/cm^2/s during 1 h. The SEM micrographs of nanoparticles after neutron bombardment showed that the nanoparticles remained spherical and separated but slightly misshaped. These applied neutron activation conditions yielded a specific activity of about 32.5 GBq per gram of nanoparticles. Preliminary estimations allow us to think that a sole injection of 50 mg of these activated nanoparticles into a brain tumor model (4.2 cm diameter) would deliver a tumor absorbed dose of up to 47 Gy. In conclusion, these dirhenium decacarbonyl-loaded nanoparticles represent a novel promising tool for radionuclide anti-cancer therapy.

Keywords: Rhenium; Dirhenium decacarbonyl; Radioactivity; PLLA; Nanoparticles; Radionuclide; Encapsulation; Cancer

1. Introduction

Despite remarkable progresses in its treatment strategies, cancer remains a major cause of death with more than 10 million people being diagnosed annually. It is estimated that there will be about 15 million new cases every year by 2020 [1]. The use of nuclear medicine in oncology is greatly contributing to both imaging and therapy aspects. During

* Corresponding author. LAGEP, Laboratoire d'Automatique et de Génie de Procédés, UMR CNRS 5007, Pharmaceutical Technology Department, Université Claude Bernard (Lyon1) (UCB), CPE-Lyon, Villeurbanne, France. Tel.: +33 0 4 72 43 18 93; fax: +33 0 4 72 43 16 82.
E-mail address: fessi@lagep.univ-lyon1.fr (H. Fessi).

0939-6411/$ - see front matter © 2007 Elsevier B.V. All rights reserved.
doi:10.1016/j.ejpb.2007.04.003

the last decade, major progress has been made in the treatment of disease with radioisotopes. Therapies and diagnosis involving the use of medical isotopes are gaining an increased interest in the race against many types of cancer [2–4]. In nuclear medicine, two general types of radiotherapy can be performed to treat cancerous tissues; (i) external radiotherapy, which unfortunately often causes radionecrosis of the surrounding healthy tissues, as well results in various side effects and several major complications [5]. (ii) the radionuclide therapy which implies the use of radioisotopes such as holmium (^{166}Ho), yttrium (^{90}Y) and rhenium (^{186}Re, ^{188}Re) in a manner to accurately restrict the radiation to a localised tumor area. In this context, the development in the nanotechnology field has been recently exploited in the elaboration of different β-emitting radioisotopes delivery vectors like liposomes [6–8], microparticles [9–11] and nanoparticles [12,13].

These radioisotopes carriers can be prepared by two general methods including: (1) Labelling vectors like liposomes [8] or albumin [12] with the isotope in its radioactive state. (2) Incorporating the isotope in its nonradioactive state into the vectors for a subsequent neutron irradiation immediately before injection to patient. Among the available neutron irradiatable vectors we find the glass microparticles (Therasphere®, MDS Nordion, USA) designed for hepatic cancer therapy [11]. Unfortunately, these yttrium-loaded glass microspheres are not biodegradable and may thus remain in the tissue long after the radioisotope is totally decayed [14]. Furthermore, these glass-based microparticles have a high density rendering their injection problematic and raising problems of settling after injection [15].

As an alternative neutron irradiatable vector, the polylactide polymer (PLLA), being a biodegradable and biocompatible polymer with interesting semi-crystalline properties, has been recently chosen as a matrix for microparticles incorporating the neutron-activatable ^{165}holmium-complexes [9] or metallic $^{185–187}$rhenium [14].

Among the most promising radioisotopes for a radionuclide therapy, we can find the rhenium ^{186}Re and ^{188}Re which can be obtained from the neutron activation of the natural rhenium which consists of the two ^{185}Re (37.4%) and ^{187}Re (62.6%) isotopes. The two radioisotopes have similar radiobiological properties and therefore do not need to be separated [14] and possess the following advantages: (1) The neutron cross-section values of the ^{185}Re and ^{187}Re (112 and 76 barn, respectively) are relatively higher than those of ^{89}Y and ^{165}Ho (1.3 and 64 barn, respectively) which implies a shorter activation time and a less costly process in the case of rhenium. (2) The maximum beta energy of ^{186}Re and ^{188}Re is 1069.5 and 2120.4 keV, being relatively high and sufficient for a radionuclide therapy. (3) The physical half-lives of ^{186}Re and ^{188}Re are 89 and 17 h, respectively, being very interesting from both a radiotherapy safety and a transport feasibility points of view. (4) The maximum tissue diffusion range of radiation for ^{186}Re and ^{188}Re is 5 and 11 mm, respectively, which satisfies an internal radiotherapy application aim. (5) Finally, both ^{186}Re and ^{188}Re emit γ lines at energy levels of (137.2 and 155 keV, respectively) [16], very similar to that of the 140 keV line of ^{99m}Tc, the frequently utilised radioisotope as a diagnostic tool in nuclear medicine.

Recently, the group of Dr. Henri Mehier, from Cerma company, France, has invented a new promising technique for a multimodal anticancer therapy and it was called targeted multi therapy (TMT) [17]. The first purpose of this technique is to treat solid tumors like, among others, brain, hepatic and pancreatic tumors by thermoablation. This thermoablation is carried out by the administration of a hot vaporised water at 400 °C under a 400 bar pressure being attained by a hydropneumatic pump. Pulses of hot water vapour are injected though a microtube being perforated with several narrow halls of some microns [18]. This approach allows solid tumors, with volume and anatomical positions not accessible to other techniques (cryoablation, radiofrequency ablation, laser ablation) to be effectively treated. The efficacy of TMT technique-mediated thermonecrosis has already been proven for treatment of cancers in animals [17–19].

In this context, our anticipated strategy would be to combine two different anticancer treatment modalities; in a first step, the thermoablation inducing a reduction of the tumor volume; and in a second step, the brachytherapy by a local injection of radioactive nanoparticles loaded with $^{186–188}$Re, via the same microtube. Indeed, many clinicians' investigations in oncology have recommended a multimodal therapy in cancer treatment to improve the treatment outcome [20,21].

In fact, anticancer drug injections are currently carried out classically by a syringe-needle system as in the intramuscular injections. Unfortunately, the drug remains concentrated at the injection site leading to a poor drug diffusion in targeted organs and a fast resumption by blood circulation. With TMT technology, under high pressure, the nanoparticles, having a nanometric size, can be propelled into the target zone and spread out over a diameter of 20 mm around the extremity of the microtube [19]. The main limitation of the innovative brachytherapy technique described here is that it is only available for solid tumors and is not easy to treat disseminated tumor cells [22].

In this framework, the goal of this study is to elaborate $^{186–188}$Re radioactive poly-lactide-based nanoparticles (NPs) which can be suitable for a radionuclide intratumoral injection by the TMT technique. These nanoparticles are designed to be dispensed in patient-ready doses that only require to be activated by a neutron radiation yielding a therapeutic amount of radioactivity and are ready for an intra-tumoral injection without any additional long handling. These nanoparticles have been prepared by an emulsion–solvent evaporation method. A 3^3 factorial design method was applied to study the influence of the different proceeding and formulation parameters on both the nanoparticles size and the rhenium encapsulation efficacy. Furthermore, different methods were used to characterize

the obtained nanoparticles including; SEM, TEM, EDS, XPS, FT-IR, RMN and DSC. Finally the results of the neutron activation of nanoparticles in nuclear reactor facilities are shown and discussed from a radionuclide therapy point of view.

2. Materials and methods

2.1. Materials

The PLLA polymer (Resomer Condensate L Mn 1900 ($M_w = 6$ kDa)) was kindly supplied by Boehringer Ingelheim, Germany. Dirhenium decacarbonyl, $Re_2(CO)10^{10}$, Poly(vinyl alcohol) (PVA, $M_w = 31$ kDa, hydrolyzation degree = 88%), boric acid, potassium iodide and iodine were all products of Aldrich, France. Dichloromethane (DCM) was from Laurylab, France. Nitric acid (65%), hydrochloric acid (12 M), sulphuric acid (95%) and sodium hydroxide (pellets) were purchased from Carlo-Erba, France.

2.2. Nanoparticles preparation

Rhenium-loaded nanoparticles (NPs) have been prepared by an oil-in-water simple emulsion–solvent evaporation method as described by Hamoudeh et al. [23] with modification. The oil-in-water emulsion consisted of:

- *Organic phase*. $Re_2(CO)_{10}$ was mixed with the polymer under different ratios in dichloromethane (DCM).
- *Aqueous phase*. Poly(vinyl alcohol) (PVA) was dissolved in continuously stirred water at 40 °C and poured into a glass beaker after cooling. PVA was used at different percentages ranging from 1% to 3% w/v. The organic phase was then added into the aqueous one under mechanical stirring (Ultraturax T25, IKA, Germany) at a defined stirring speed for 2 min. The stirring speed ranged between 11,000 and 24,000 rpm.

After obtaining the emulsion, DCM was evaporated by a rotative evaporator (R-144, Buchi, Switzerland) at 100 rpm for 15 min under vacuum. The prepared nanoparticles were separated by ultracentrifugation (Beckman, USA) and then washed with water several times to eliminate the excess of PVA.

Finally, 1 ml of NPs suspension was filled into 5 ml freeze-drying vials. The freeze-drying of nanoparticles was performed using a pilot freeze-dryer; Usifroid SMH45 (Usifroid, France). It consists mainly of three stainless steel shelf Plates (3×0.15 m^2), a coiled tube used as a condenser at -65 ± 5 °C and a vacuum pump. The conditions applied during the present study were: freezing for 2 h at -50 °C with a temperature ramp of 1 °C/min, sublimation at -40 °C and 60 μbar for 15 h and finally the secondary drying was carried out at 25 °C and 50 μbar for 4 h.

Furthermore, $Re_2(CO)_{10}$-loaded films at different rhenium loadings, ranging from 0% to 24% w/w (ICP-AES results, data not shown), have been prepared by dissolving different amounts of the polymer and $Re_2(CO)_{10}$ in DCM. The solutions were cast thereafter onto a flat glass plate followed by solvent evaporation at room temperature during 48 h.

2.3. Rhenium loading and encapsulation efficacy determination

The titration of rhenium was performed on a spectrometer ARL 3580 (Thermo, USA) based on inductively coupled plasma atomic emission (ICP-AES). A sample of 20 mg of prepared nanoparticles was digested in a medium containing 1 volume of H_2SO_4 (95%) and 2 volumes of fuming HNO_3 (68%). The assay was linear between 0 and 10 μg (metallic rhenium)/ml with a correlation coefficient of 0.999. To calculate the encapsulation efficacy, we used the theoretical $Re_2(CO)_{10}$-loading, being the used amount of $Re_2(CO)_{10}$ per 100 mg of prepared NPs. $Re_2(CO)_{10}$ encapsulation efficacy $\% = 100 \times$ (experimental loading/theoretical loading).

2.4. Size determination

The size of the obtained nanoparticles was determined by photon correlation spectroscopy (PCS) using Zetasizer 3000 HSa (Malvern, England) at 25 °C. Two to three drops of nanoparticles suspensions were diluted in 3 ml of distilled water. Each measurement was performed in triplicate.

2.5. Scanning electronic microscopy (SEM)

NPs suspensions were deposited on a metallic probe then metallized with gold/palladium with a cathodic pulverizer technics Hummer II (6 V, 10 mA). Imaging was realized on a FEG Hitachi S800 SEM at an accelerating voltage of 15 kV.

2.6. Transmission electronic microscopy (TEM)

NPs suspensions were visualised using a Philips CM120 TEM. The suspensions were placed on a carbon-coated copper TEM grid, without staining, and then allowed to air-dry before TEM viewing.

2.7. Energy dispersive X-ray spectrometer (EDS)

EDS assay was also performed to obtain a comprehensive analysis of the elemental structure of $Re_2(CO)_{10}$-loaded nanoparticles. The assays were carried out using an electronic microprobe (Camebax, Cameca Instruments, France). For this test, a small amount of lyophilised nanoparticles was placed on a carbon-coated copper TEM grid. In each analysis, the probed zone was a square of a few hundreds of μm on side. Five measurements were carried out in different zones of the sample.

2.8. X-ray photoelectron spectroscopy (XPS)

Surface analysis was carried out using a SSI probe. XPS analyses were performed on lyophilised nanoparticles for C1s, O1s, Re 4f7/2 and Re 4f5/2 peaks using a non-monochromatized Al Kα X-ray source.

2.9. X-ray diffraction (XRD)

X-ray powder diffractometry analysis was carried out to investigate the effect of the microencapsulation process on the crystalline properties of both the polymer and $Re_2(CO)_{10}$. The XRD patterns were recorded on a Siemens D500 operated with Cu Kα × radiation, a voltage of 40 kV and a current of 30 mA. The scans were conducted at a scanning rate of 1° min^{-1} in the 2θ range from 5° to 65°.

2.10. Fourier transformed infra-red (FT-IR)

The nanoparticles, the polymer, $Re_2(CO)_{10}$ and physical mixtures were characterized by infra-red spectroscopy using a Unicam Mattson 5000 FT-IR spectrometer at room temperature. Samples were crushed in a mortar, mixed thoroughly with powdered KBr to about 1% by weight and pressed to form a transparent pellet. The spectra were taken in the KBr pellets in the range of 3500–400 cm^{-1}.

2.11. NMR characterization

^1H and ^{13}C and NMR spectra of the polymer, the $Re_2(CO)_{10}$ and the lyophilised $Re_2(CO)_{10}$-loaded nanoparticles were acquired on a Bruker DMX-300 SB spectrometer in chloroform $CDCl_3$. In each analysis, about 25 mg of samples was placed into 5 mm NMR tubes, and then was dissolved in 2 ml of $CDCl_3$.

2.12. Differential scanning calorimetry (DSC)

Thermal analysis was performed using a differential scanning calorimeter DSC TA 125 (TA instrument USA). Samples powders (5–10 mg) were introduced into aluminium pans and was hermetically sealed. All samples were heated at a 2 °C min^{-1} scanning rate between 25 and 200 °C after a 5 min stabilisation period under nitrogen. Thermograms are expressed in °C = f(mW). Pure PLLA and $Re_2(CO)_{10}$ were used as controls. The instrument was calibrated with indium for melting point and enthalpy heat of melting heat.

2.13. Determination of poly(vinyl alcohol)

The residual amount of PVA in the obtained nanoparticles was determined using an iodine-borate colorimetric method described by Zielhuis et al. [24] with some modification. The method involves the extraction of polyvinyl alcohol from the sample matrix into an aqueous phase, followed by the formation of a PVA–iodine–borate complex that can be detected by visible spectroscopy. The method consists of solubilizing PVA by destroying the nanoparticles (50 mg) with 2 ml of 1 M NaOH for 30 min at 90 °C. The resulting solution was neutralized with 1 M HCl. Then, 3 ml of a boric acid solution (3.7% w/v) and 0.5 ml of an iodine solution (1.66% KI + 1.27% I_2 in distilled water) were added and the volume was adjusted to 10 ml with distilled water. Samples were analysed at 680 nm using a Cary 50 spectrophotometer (Varian, Australia) in triplicate. Known amounts of PVA added to 50 mg of PLLA were treated in the same way and used as standards. The correlation coefficient for the given standards of PVA was 0.988.

2.14. Factorial design

The influence of the different process parameters on both the nanoparticles size and the $Re_2(CO)_{10}$ encapsulation efficacy has been investigated by an experimental design methodology. In our objectives, the experimental design was chosen to support a quadratic regression model as adequate to estimate a potentially complex response function

$$Y = b_0 + b_1X_1 + b_2X_2 + b_3X_3 + b_{11}X_1^2 + b_{22}X_2^2 + b_{33}X_3^2 + b_{12}X_1X_2 + b_{13}X_1X_3 + b_{23}X_2X_3 + b_{123}X_1X_2X_3, \quad (1)$$

where Y is the simulation model response, b_0 is the arithmetic mean response of runs, b_1, b_2 and b_3 are the estimated linear coefficients for the factors X_1, X_2 and X_3, b_{11}, b_{22}, b_{33} are the quadratic coefficients and b_{12}, b_{13}, b_{23}, b_{123} are the interaction coefficients. Then, the different parameters' influences were studied by a D-optimal design approach. The D-optimal design was computed by Modde (Version 6 Umetrics AB, Sweden) in 18 experiments. G-efficiency criterion was used to select the optimal worksheet design set. Finally, run sequence of experimental units was completely randomized to minimize the effect of noise and then keeping out the experiment from systematic bias. For each factor, the lower, center and higher levels can be presented by a −1, 0 and 1 sign, which is shown in Table 1. To obtain a clearer view, the formula used in the factorial design can also be presented in a cube shape, where the different axes constitute the different variables (Fig. 1).

2.15. Thermal neutron activation analysis (NAA)

The rhenium content of nanoparticles has been also determined by neutron activation analysis using a low neu-

Table 1
Sitting levels for chosen variables

Independent variables	Code	−1	0	+1
(X_1) stirring speed (rpm)	SPD	11,000	17,500	24,000
(X_2) polymer concentration (% w/v)	PLA	2	3	4
(X_3) PVA concentration (% w/v)	PVA	1	2	3

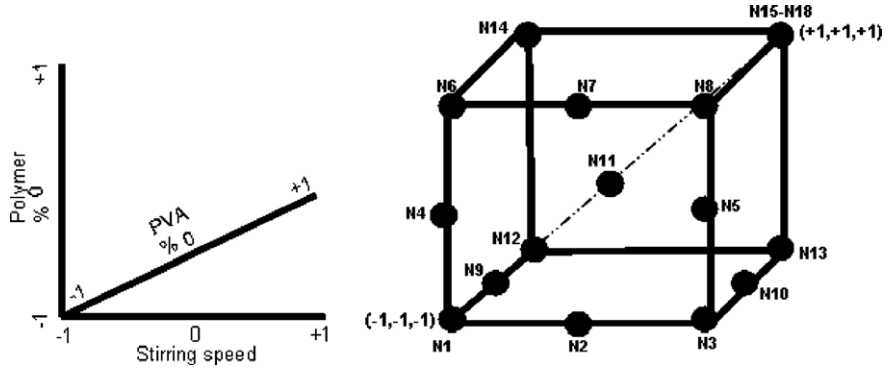

Fig. 1. The factorial design represented by a cube in which the three axes constitute the three different variables at the three described levels.

tron flux facility (1×10^{11} n/cm^2/s) for 30 min. Each radioactive nuclide that is formed during irradiation decays with a specific half-life, emitting gamma rays of characteristic energy. The energy of delayed gamma rays is used to determine which elements are present in the sample, and the amount of the obtained specific energy is used to determine the weight percentage of these elements in the sample. Subsequent to irradiation, gamma ray induced activity in the samples is measured with a high resolution spectrometric system using high purity germanium (HpGe) detector. About five determinations have been realized for each sample.

2.16. Neutron activation

All irradiations were performed in the TRIGA reactor facilities in Pitesti, Romania. For our purposes we used the irradiation channel with a thermal neutron flux of 1.45×10^{13} n/cm^2/s for 1 h. Irradiation was carried out in a sealed poly-propylene cylinder. The specific activity of the samples at the end of irradiation is calculated using the following equation

$$\Lambda = \phi \cdot n \cdot \frac{\left[\sigma_0 + \frac{1}{f} \cdot I_0\right] \cdot (1 - \exp(-\lambda \cdot \mathrm{TIR})) \cdot \exp(-\lambda \cdot \mathrm{TR})}{k \cdot m} \quad (2)$$

where: Λ is the specific activity (μCi/g), Φ is the thermal neutron flux (n/cm^{2}s) (neutrons with $E < 0.5$ eV) is the 1.04×10^{13} n/cm^2/s, n is the number of target nuclei in the irradiated sample (^{185}Re or ^{187}Re);

$$n := m \cdot Ab \cdot \frac{\mathrm{NA} \cdot p}{A}$$

NA is the Avogadro's number, A is the atomic mass (185; 187), p is the rhenium concentration in the sample (% w/w), σ_0 is the thermal neutron cross-section (cm^2), f is the thermal to epithermal neutron flux ratio, I_0 is the effective resonance integral (cm^2), λ is the decay constant which equals $\ln(2)/T_{1/2}$ (s^{-1}), TIR is the irradiation time (s), TR is the cooling time after irradiation (s) being 0 in our case, k is the 3.7×10^4, m is the sample weight (g).

3. Results and discussion

3.1. Rhenium-loaded nanoparticles preparation by a factorial design method

The classical approach used in microparticles and nanoparticles elaboration studies, where one factor is varied whilst the others remain constant, is unlikely to reveal the possible presence of inter-factors interactions [25]. A factorial design is frequently employed as a research planning tool because it provides the maximum information, requiring the least experiments [26,27]. In this way, factorial design enables all factors to be varied simultaneously, allowing quantification of the effects caused by independent variables and the eventual interactions between them. In this study, an orthogonal experimental design was introduced to optimize the formulation of $Re_2(CO)_{10}$-loaded nanoparticles. In order to optimize the preparation of nanoparticles, the stirring speed (X_1), the polymer concentration (X_2), and the PVA concentration (X_3) were chosen as independent variables. The final selection of these three variables was based on the results of preliminary investigations which included aside from these three variables, the volumes of both internal and external emulsion phases, the evaporation method and the stirring time, being finally excluded as they did not show a clear influence on the investigated responses. Furthermore, the range of each variable would be chosen in order to adequately measure its effects on the studied response. These ranges must be also chosen so that they encompass all of the preparation conditions likely to be encountered during nanoparticles preparation process (Table 2).

The two responses (nanoparticles sizes and encapsulation efficacy) were calculated and applied as regressors in a PLS correlation [28], using the starting settings as descriptor matrix at a confidence level of 0.95. The analysis of data was carried out using ANOVA, and the individual parameters were evaluated with F test.

Table 2
The factorial design generated combinations (in orthogonal values)

Run	X_1	X_2	X_3
1	−1	−1	−1
2	0	−1	−1
3	+1	−1	−1
4	−1	0	−1
5	+1	+1	−1
6	−1	0	−1
7	0	+	−1
8	+1	+1	−1
9	−1	−1	0
10	+1	−1	0
11	0	0	0
12	−1	−1	+1
13	1	−1	+1
14	−1	+1	+1
15*	+1	+1	+1
16*	+1	+1	+1
17*	+1	+1	+1
18*	+1	+1	+1

Asterisk (*) denotes combinations carried more than once for the reproducibility study.

3.1.1. Nanoparticles size

The particles size is an important parameter, as it can influence the biopharmaceutical properties and the fate of nanoparticles. The summary of model fit (Fig. 2) showed that our model was acceptable for the nanoparticles size response with both high model accuracy (R^2) and predictability (Q^2); 0.98 and 0.80, respectively. Furthermore, the model validity and reproducibility are 0.53 and 0.99, respectively. The correlation coefficient for the nanoparticles size response is shown in (Fig. 3). As it can be seen, a good correlation between predicted and experimental response was observed for nanoparticles size. With a particles size ranging between 330 and 1500 nm, the polynomial correlation given by the model for the nanoparticles size response was as follows:

$$\begin{aligned}\text{Np size(nm)} = {} & 606.7 - 348.1\text{SS} + 125.5\text{PLA} \\ & - 45.1\text{PVA} + 129.1\text{SS}^2 + 53.4\text{PLA}^2 \\ & - 35.5\text{PVA}^2 - 66.8\text{SS.PLA} \\ & + 27\text{SS.PVA} + 1.9\text{PLA.PVA} \\ & - 15.6\text{SS.PLA.PVA} \end{aligned} \quad (3)$$

As it can be noticed from Fig. 4, the most dominant factor concerning the nanoparticles size was the stirring speed. The nanoparticles size is visible in the plane of the surface plot that slopes downwards towards higher stirring speeds whatever be the utilised polymer or PVA concentrations. This clear negative effect of stirring rate on the nanoparticles size has been widely mentioned in the literature [23,29–32]. Generally, authors explain this negative effect by the fact that the higher the applied stirring speed in the system, the more available energy to disperse the oily phase in the aqueous one yielding smaller droplets and resulting in smaller nanoparticles.

Furthermore, the polymer concentration in the oily phase has been shown to have a positive influence on the nanoparticles size (Fig. 4). This effect was also remarkably noticed whatever the applied stirring speeds or the PVA concentrations. Thus, larger nanoparticles sizes could be obtained with higher polymer concentration. This is in agreement with other published papers [23,29,32–37]. Indeed, the higher concentration of polymer in the oily phase probably causes an increase in the viscosity of this last phase rendering it more resistant to shear forces [38].

In contrary, the PVA concentration in the external aqueous phase has a relatively negative influence but however less clear than the stirring speed's one (Fig. 4). Indeed, the PVA-induced particles size reduction has been frequently mentioned in the literature [29,32,39] and it was explained by the fact that the increase in PVA concentrations would render the external aqueous phase more viscous, which intensifies the shear forces' impact on the oily phase and allows obtaining smaller emulsion droplets.

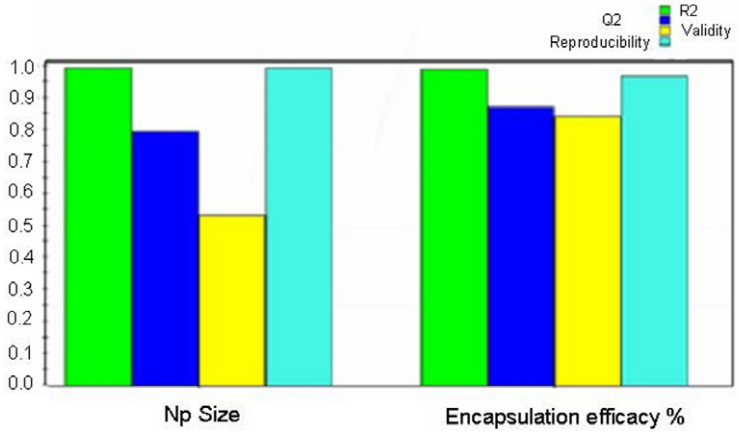

Fig. 2. Summary of fit showing from left to right model accuracy (R^2), model predictability (Q^2), model validity and reproducibility, respectively, for both nanoparticles size and $Re_2(CO)_{10}$ encapsulation efficacy (EE) responses.

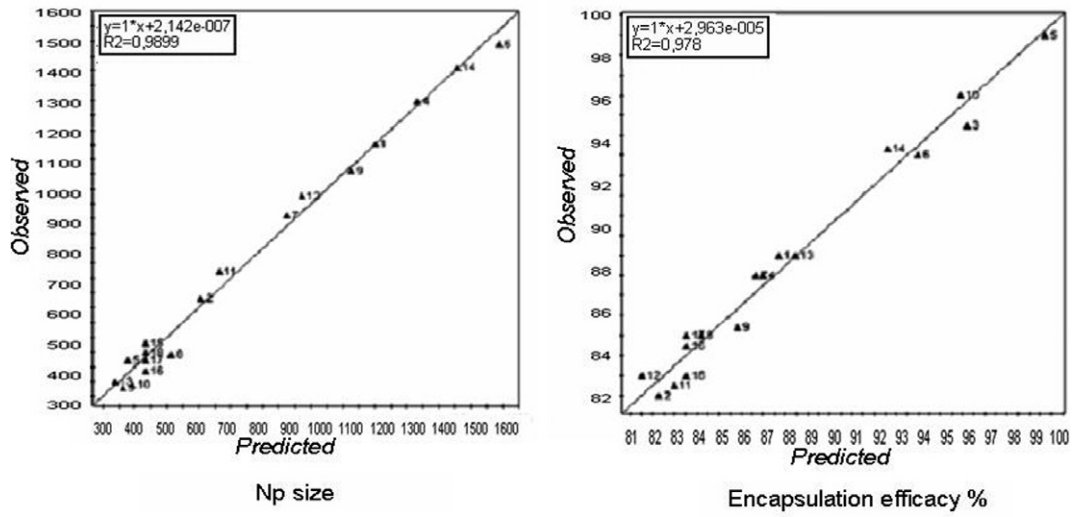

Fig. 3. Predicted versus experimental data for each of the two studied responses.

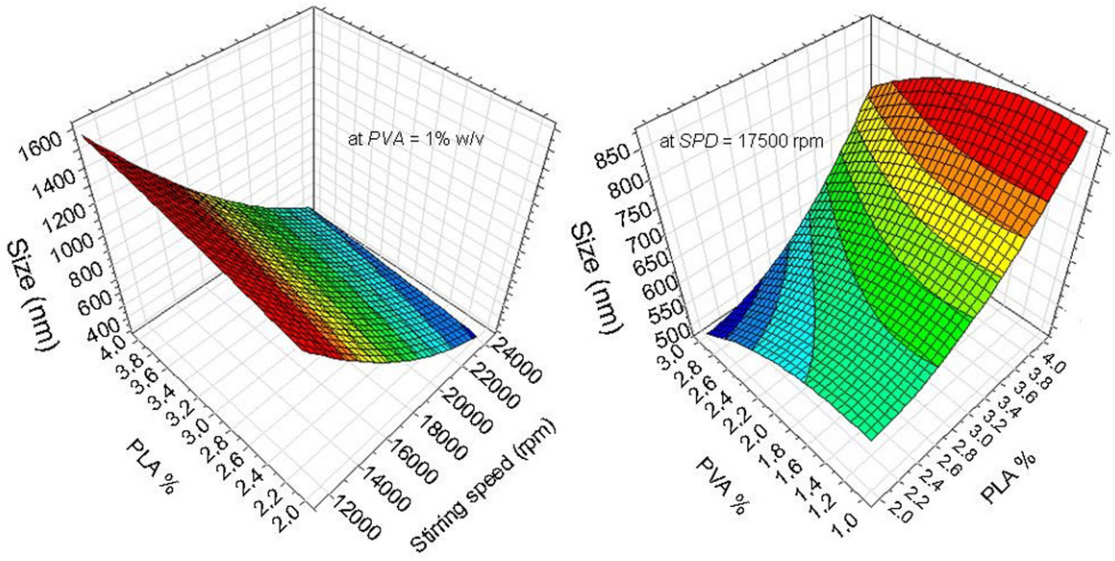

Fig. 4. Response surface plot for the nanoparticles size. Different formulation variables are presented in the different axes.

3.1.2. Dirhenium decacarbonyl encapsulation efficacy

In the field of nanotechnology, drug encapsulation efficacy is an important index to characterize drug delivery systems. In the case of rhenium-loaded nanoparticles which are designed for a further neutron bombardment, higher rhenium loadings within nanoparticles enable getting higher radiotherapeutic doses at relatively shorter activation times [14,40]. Here, the encapsulation efficacy ranged between 81% and 98% yielding rhenium metal loadings of 13–24% mg (Re metal)/mg (nanoparticles).

The summary of model fit (Fig. 2) showed that our model was also acceptable for the $Re_2(CO)_{10}$ encapsulation efficacy response with high model accuracy (R^2), predictability (Q^2), validity and reproducibility; 0.98, 0.87, 0.84 and 0.96, respectively. The correlation coefficient for the $Re_2(CO)_{10}$ encapsulation efficacy response is shown in (Fig. 3). As it can be noticed, a good correlation between predicted and experimental response was observed. The polynomial correlation given by the model for the rhenium encapsulation efficacy response was the following:

$$\begin{aligned} &Re_2(CO)_{10}\ \text{encapsulation efficacy}(\%) \\ &\quad = 88.4 - 3.4SS + 2.68PLA - 1.48PVA + 0.35SS^2 \\ &\qquad - 2.08PLA^2 + 0.14PVA^2 - 1.7SS.PLA \\ &\qquad + 0.65SS.PVA - 0.57PLA.PVA \\ &\qquad - 0.37SS.PLA.PVA \end{aligned} \quad (4)$$

Fig. 5 shows the general trends of the $Re_2(CO)_{10}$ encapsulation efficacy response toward the simultaneous changes of the three different parameters. From the figure, it can be noticed that the most influential parameter has been the polymer concentration in the oily phase which has a positive impact on the encapsulation efficacy whatever be the

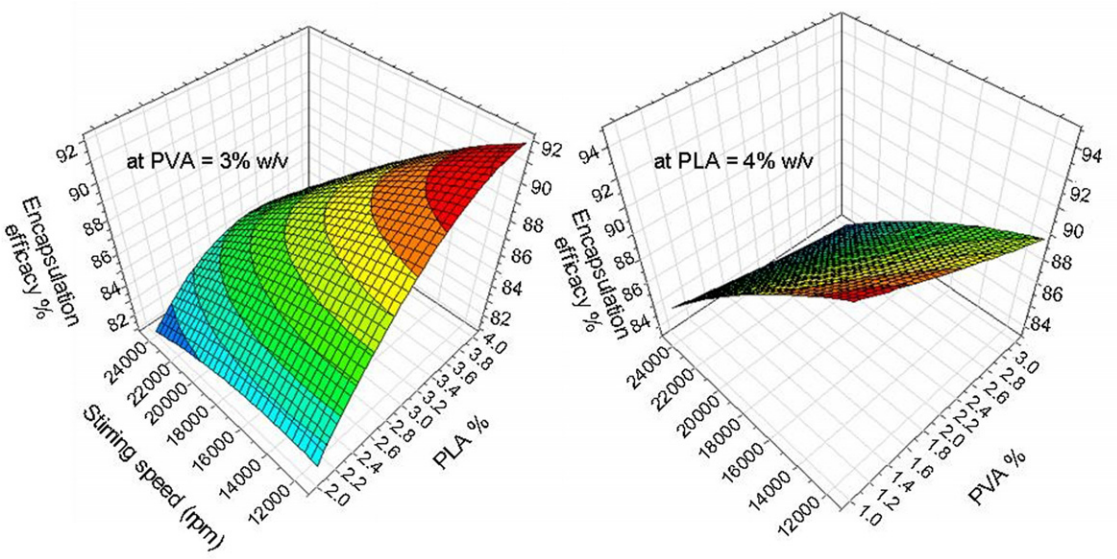

Fig. 5. Response surface plot for the dirhenium decacarbonyl encapsulation efficacy. Different formulation variables are presented in the different axes.

two other parameters. This would mean that the $Re_2(CO)_{10}$ encapsulation yield increased (from 81% to 98%) when the amount of polymer increases in the formulae. In accordance with the results of Gorner et al. [41], we can explain this tendency by the fact that as shown above, higher PLLA amount in the organic phase leads to larger nanoparticles and as the nanoparticles diameter increase is related to a relative decrease of the surface area, this would reduce the possibility of $Re_2(CO)_{10}$ molecules loss by diffusion towards the suspending aqueous medium during the emulsification and the further solvent evaporation. Our results are in accordance with other published data concerning the encapsulation of lipophilic molecules [35,41–43]. For instance, Chen et al. [42] reported a lidocaine encapsulation yield increasing from 8% to 35% after doubling the PLLA concentration in the organic phase in a solvent evaporation-like method.

Concerning the two other parameters, the stirring speed and the PVA concentration, it was found that they both had a negative effect on the encapsulation efficiency (Fig. 5) which is in agreement with other published works [44,45]. However, their effect being small and insignificant became clearer when higher polymer concentrations were applied. For instance, when combining simultaneously higher stirring speeds with higher PVA concentrations, the encapsulation efficacy decreased from 98% to 82% (16 units) at higher PLLA concentration (4% w/v) while it decreased only from 87% to 81% (6 units) at lower PLLA concentration (2% w/v). Indeed, as it can be understood, contrary to the PLLA effect, the increase in either the stirring speed or the PVA concentration would lead to a decrease in the size as mentioned above, which is accompanied by an increase in the nanoparticles surface area per unit of volume and by consequence a probable raised chance of a $Re_2(CO)_{10}$ molecules loss by diffusion towards the external aqueous phase. Furthermore, as proposed by Feng et al. [45] for the lipophilic paclitaxel molecule, the resulting reduction in the $Re_2(CO)_{10}$ encapsulation efficacy may be attributed partially to the fact that some $Re_2(CO)_{10}$ molecules may bind to the excessive PVA molecules in the system which induces a leaching out of $Re_2(CO)_{10}$ molecules during the fabrication procedure. It can thus be concluded that the presence of an optimal amount of the emulsifier used in the fabrication process for the encapsulation efficiency is justifiable from both optimal encapsulation yield and safety points of view. Therefore, the residual amount of PVA absorbed onto the nanoparticles surface has been monitored by a colorimetric titration as explained above. We could find less than 2% w/w of PVA in the nanoparticles which is frequently reported elsewhere [23,39,46–48]. Furthermore, the residual amount was found to increase slightly with the amount used in formulation which is in accordance with the results of Sahoo et al. [39] who showed the PVA molecules remaining in the composition of the nanoparticles after preparation and to be very difficult to be eliminated from the nanoparticles surface [47].

3.2. Rhenium-loaded nanoparticles characterization

3.2.1. Electronic microscopy images

Figs. 6 and 7 show the SEM and TEM micrographs of rhenium-loaded nanoparticles. As it can be seen, they are spherical with a relatively small index of polydispersity (between 0.1 and 0.2) according to the photon correlation spectroscopy (PCS) results.

3.2.2. Elemental analysis and surface study

The elemental analysis of rhenium-loaded nanoparticles loaded with 23% w/w rhenium, as determined by ICP-AES, has been conducted using EDS technique. The elemental analysis results are shown in Table 3. As it can be noticed, the elemental rhenium weight percentage was confirmed to be around 23% w/w by analysing different zones of nano-

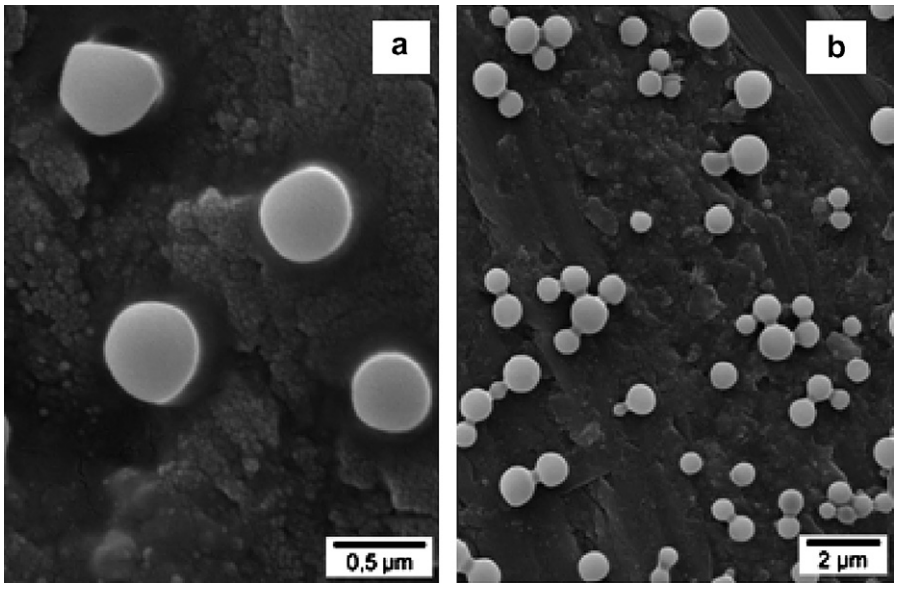

Fig. 6. SEM micrograph of rhenium-loaded nanoparticles (bar = 0.5 μm (a), 2 μm (b)).

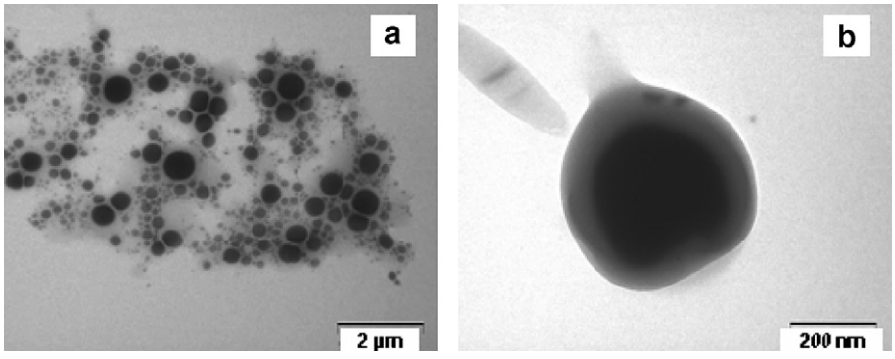

Fig. 7. TEM micrograph of rhenium-loaded nanoparticles (bar = 2 μm (a), 0.2 μm (b)).

Table 3
EDS elemental analysis of re-loaded nanoparticles at 23% Re w/w as determined by ICP-AES

Element	Atom %	Weight %	Weight % error
C	59.48	41.16	0.90
O	38.33	35.32	1.18
Re	2.19	23.52	0.65

particles preparations. Also, Fig. 8a shows the elemental composition of the rhenium-loaded nanoparticles.

To investigate the distribution of rhenium within the nanoparticles, XPS assay (Fig. 8b) has been performed and the results showed the presence of less than 1% w/w at the surface of nanoparticles at up to 10 nm analysed surface thickness indicating the success of the encapsulation of

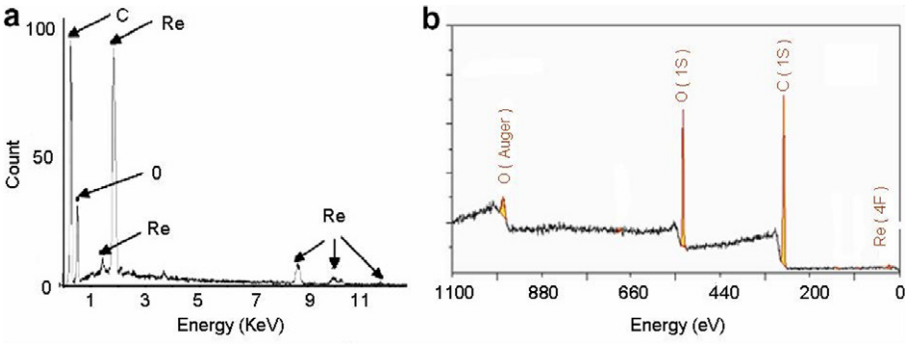

Fig. 8. (a) EDS elemental analysis of rhenium-loaded nanoparticles, (b) XPS results of rhenium-loaded nanoparticles.

$Re_2(CO)_{10}$ in the interior of nanoparticles. However, the rhenium surface concentrations could not be precisely determined as the rhenium detected peaks were very small and not far from the background count of noise. The recorded peaks for rhenium were the Re 4f7/2 at 42.1 eV and the Re 4f5/2 at 44.55 eV.

3.2.3. X-ray diffraction (XRD)

The X-ray diffraction (XRD) analyses of the PLLA, $Re_2(CO)_{10}$, blank nanoparticles and $Re_2(CO)_{10}$-loaded nanoparticles are shown in Fig. 9. The diffraction profile for the PLLA reveals the presence of peaks at 14.8°, 16.8°, 19.1°, and 22.9° which is consistent with that of peaks at 15°, 16°, 18.5°, and 22.5° reported by Xu et al. [49] and Ikada et al. [50]. These PLLA peaks were again detected in both blank and rhenium-loaded nanoparticles. The X-ray diffraction pattern of pure dirhenium decacarbonyl is also shown in Fig. 9. It can be observed that the characteristic peaks of $Re_2(CO)_{10}$ almost could be found in nanoparticles. This indicates that the $Re_2(CO)_{10}$ has kept its crystalline form after encapsulation in nanoparticles. However, the intensity of the $Re_2(CO)_{10}$ peaks was reduced perhaps because of a dilution effect as it has been explained by Tayade and Kale [51] for ibuprofen in gelatine based microparticles. Such a dilution effect has been confirmed on prepared films including different percentages of $Re_2(CO)_{10}$ and PLLA (data not shown).

3.2.4. Infra-red spectral analysis (FT-IR)

As shown in Fig. 10, there was no significant difference between the FT-IR spectra of the physical mixture of $Re_2(CO)_{10}$ and polymer as well as $Re_2(CO)_{10}$-loaded nanoparticles when compared to the spectra of individual components. The characteristic absorption peaks of PLLA are evident at about 1750 cm^{-1} (carbonyl groups), 1080 cm^{-1} (C–O–C stretching bands) and 1450 cm^{-1} (C–H stretching in methyl groups) [52,53]. The characteristic carbonyl-stretching bands of $Re_2(CO)_{10}$ at 2071, 1992 and 1975 cm^{-1}, in accordance with the values given by Firth et al. [54], were also detected in the nanoparticles indicating the stable nature of $Re_2(CO)_{10}$ after the encapsulation process. Briefly, the $Re_2(CO)_{10}$-loaded nanoparticles spectra appear as the sum of pure $Re_2(CO)_{10}$ and PLLA spectra,

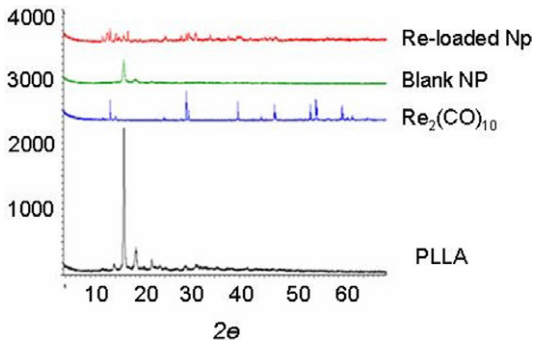

Fig. 9. The XRD of PLLA, pure dirhenium decacarbonyl, blank nanoparticles and dirhenium decacarbonyl-loaded nanoparticles.

and these experiments revealed that there was no significant interaction between $Re_2(CO)_{10}$ and PLLA.

3.2.5. NMR characterization

In this assay, we have scanned the spectra of $Re_2(CO)_{10}$, PLLA, their physical mixture and $Re_2(CO)_{10}$-loaded nanoparticles. In the proton spectra of $Re_2(CO)_{10}$-loaded nanoparticles, the characteristic peaks of PLLA are evident at 1.52–1.61 ppm (3H, d, $J = 7.15$ Hz), 5.11–5.21 ppm (1H, q, $J = 7.16$ Hz). In the carbon spectra, the characteristic carbonyl-stretching band of $Re_2(CO)_{10}$ at 169 ppm was also detected in the nanoparticles indicating the absence of interactions between the PLLA and the $Re_2(CO)_{10}$ after encapsulation process. Thus, in accordance with the FT-IR results, the $Re_2(CO)_{10}$-loaded nanoparticles spectra appear as the sum of both pure $Re_2(CO)_{10}$ and PLLA spectra.

3.2.6. Differential scanning calorimetry (DSC)

The DSC technique has been widely applied in microencapsulation systems as a valuable characterization method to obtain both qualitative and quantitative data about the physicochemical status of the incorporated drugs in nano-microparticles [55]. Using the DSC analysis of drug, polymer materials and produced nanoparticles, the nature of the drug inside the polymer matrix can be studied, which may emerge from crystalline [51] to amorphous form [56] and can be molecularly dispersed [24] or dissolved in the polymer [57] influencing by consequence the relevant *in vitro* release properties [51].

The thermal curves of pure components; $Re_2(CO)_{10}$, PLLA and of 23% w/w loaded $Re_2(CO)_{10}$ nanoparticles are presented in Fig. 11. The PLLA thermal curve showed a transition temperature of about 45 °C and a melting point at 142 °C with a melting enthalpy of 30 J/g. This means that our chosen polymer has a semi-crystalline nature with a degree of crystallinity of 31.5%. This last value was calculated as the percentage of its melting enthalpy over the melting enthalpy for a 100% crystalline PLLA ($\Delta H_f(100\%) = 95$ J/g) [58]. As it can be expected for a further neutron activation application, polymers having crystalline domains like PLLA would be preferable above amorphous ones like PLGA or PDLLA. Indeed, it has been shown concerning gamma rays sterilisation effects on polymer based nanoparticles, that polymer crystalline domains would be less susceptible toward radiation-induced degradation compared with amorphous ones [59]. The pure $Re_2(CO)_{10}$ thermal curve displayed two separate sharp endothermic peaks at 93 and 170 °C corresponding, respectively, to a reversible transition and to the $Re_2(CO)_{10}$ melting point as shown by Lemoine et al. [60,61]. Concerning the $Re_2(CO)_{10}$-loaded nanoparticles, these two characteristic, mentioned above, endothermic peaks of $Re_2(CO)_{10}$ appeared again at the same temperatures indicating that $Re_2(CO)_{10}$ has conserved its crystalline pattern after encapsulation in agreement with XRD results. Furthermore, we have found a clear reduction in the PLLA melting enthalpy accompanying the increase in

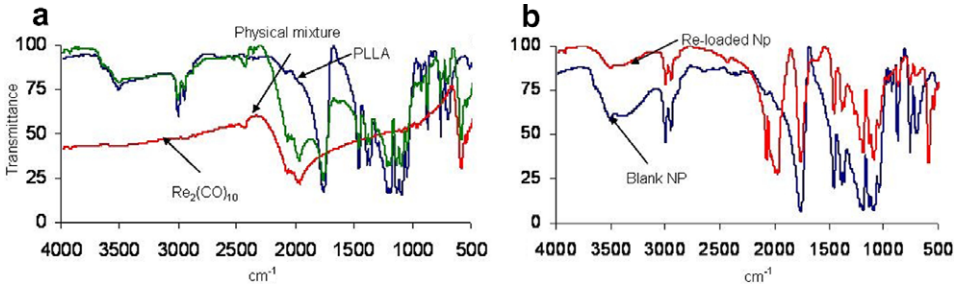

Fig. 10. (a) FT-IR results for PLLA, pure dirhenium decacarbonyl and their physical mixture. (b) FT-IR results for blank nanoparticles and dirhenium decacarbonyl-loaded nanoparticles.

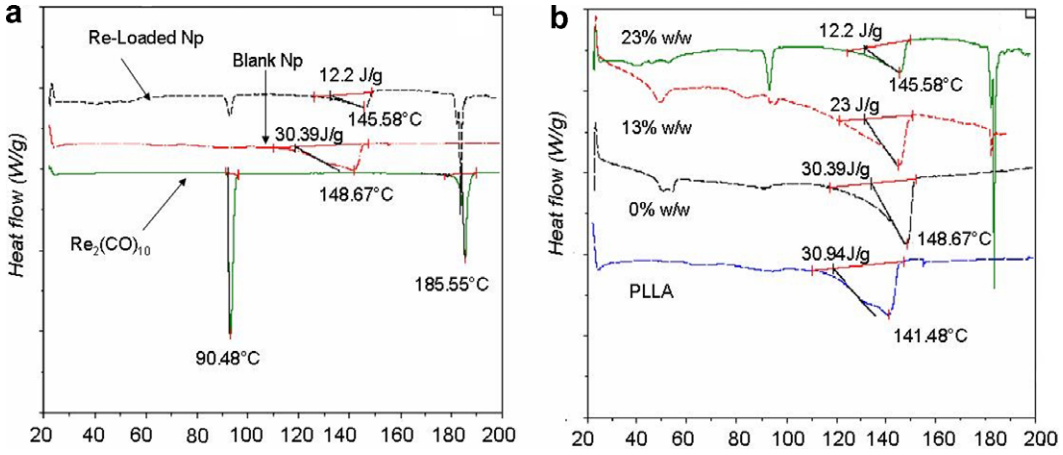

Fig. 11. (a) DSC results for pure dirhenium decacarbonyl, blank nanoparticles and dirhenium decacarbonyl-loaded nanoparticles. (b) DSC results for pure PLLA and dirhenium decacarbonyl-loaded nanoparticles at different rhenium loadings ranging from 0% to 23% w/w.

rhenium loading. As it can be noticed in Fig. 11b, the PLLA melting enthalpy decreased from 30 to 23 to 12 J/g at rhenium metal loadings of 0%, 13% and 23% w/w, respectively. This trend was also similarly found in preliminary experiments in our laboratory dealing with PCL based $Re_2(CO)_{10}$. However, DSC analyses on different films including different percentages of $Re_2(CO)_{10}$ and PLLA have confirmed the same decrease in PLLA melting enthalpy in the same trend (data not shown). Therefore, we would explain this reduction in PLLA melting enthalpy by a dilution effect due to the presence of ascending amounts of $Re_2(CO)_{10}$ within nanoparticles rather than a $Re_2(CO)_{10}$ plasticizer effect as shown by Mumper et al. [62] for holmium acetylacetonate-loaded PLLA nanoparticles.

3.3. Neutron activation

Neutron activation analysis (NAA) is an analytical technique useful for performing both qualitative and quantitative multi-element analyses in the sample of interest. Activation analysis relies on the nuclear reaction between neutrons and target nuclei. The most common type of nuclear reaction for NAA is neutron capture (*n*, gamma) reaction. When a neutron interacts with target nucleus via a non-elastic collision a nucleus forms in an excited state. This new configuration yields a radioactive nucleus which decays by emission of one or more characteristic delayed gamma rays. In our case the neutrons interact with the ^{185}Re and ^{187}Re target nucleus, thereby converting the latter into radioactive ^{186}Re and ^{188}Re nucleus (Fig. 12). As the radioactive nucleus decays back to stable state, gamma rays are emitted, and the amount of emitted radiation depends on the number of atoms in the target sample.

The rhenium content in nanoparticles has been determined many times for each sample and at different cooling times after activation. Fig. 12 shows the gamma energy emitted from both ^{186}Re and ^{188}Re nucleus after about 118 h of activation which is equal to 1.32 and 7 times the half-lives of ^{186}Re and ^{188}Re, respectively. Logically, at this elapsed period after activation, the remained gamma energy levels of ^{186}Re became relatively higher than those of ^{188}Re.

Furthermore, from Table 4 in which are presented the results of rhenium titration by both ICP-AES and NAA in some nanoparticles samples, it can be noticed that the rhenium element loadings determined by NAA coincided very well with those determined by ICP-AES.

Fig. 13 shows the nanoparticles after neutron irradiation at both neutron fluxes (1×10^{11} and 1.45×10^{13} n/cm^2/s). It can be noticed that nanoparticles kept their spherical shape at the lower neutron flux used for NAA determination while at the higher one, some nanoparticles appear to be misshaped spheres but remained separated and rarely agglomerated. However, this should not negatively influ-

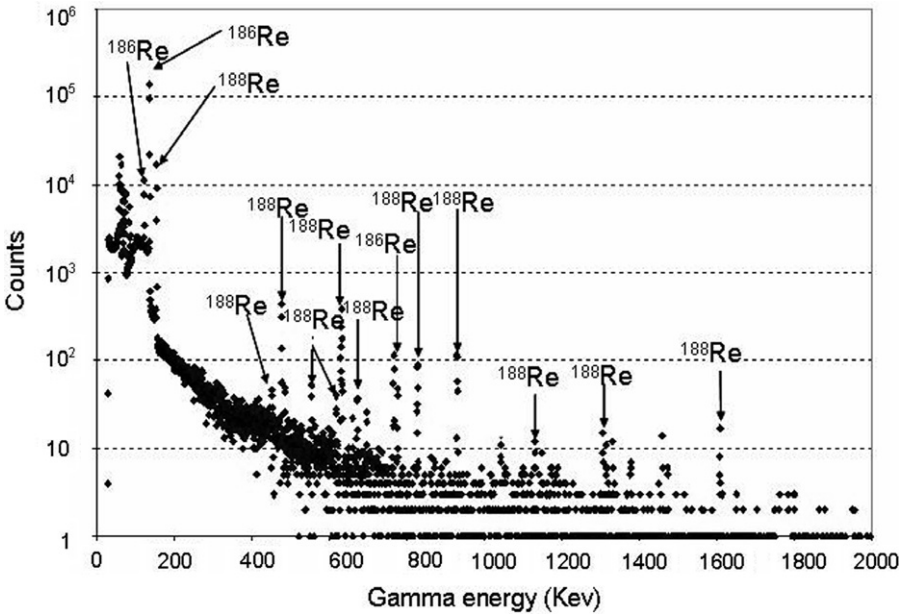

Fig. 12. The gamma rays emitted by ^{186}Re and ^{188}Re of activated nanoparticles at 117 h elapsed time after irradiation.

Table 4
A comparison between the rhenium loading determinations between ICP-AES and NAA methods

Sample	Rhenium % w/w (ICP-AES)	Re % w/w (NAA)	(ICP-AES)/(NAA)
A	19.5	18.91	1.03
B	21.3	20.97	1.01
C	13.8	13.05	1.05
D	23.37	23.26	1.005
E	20.97	20.8	1.008

ence the final usage of these nanoparticles as they remained redispersible in water, phosphate buffer solution or physiologic serum after short ultrasonication or vertoxing for a subsequent injection. Actually, different characterization studies are being performed in our laboratory to evaluate the irradiation impact on the chemical composition and the physical integrity of these $Re_2(CO)_{10}$-loaded nanoparticles.

Furthermore, to obtain radioactive doses, different batches of nanoparticles have been activated at a high neu-

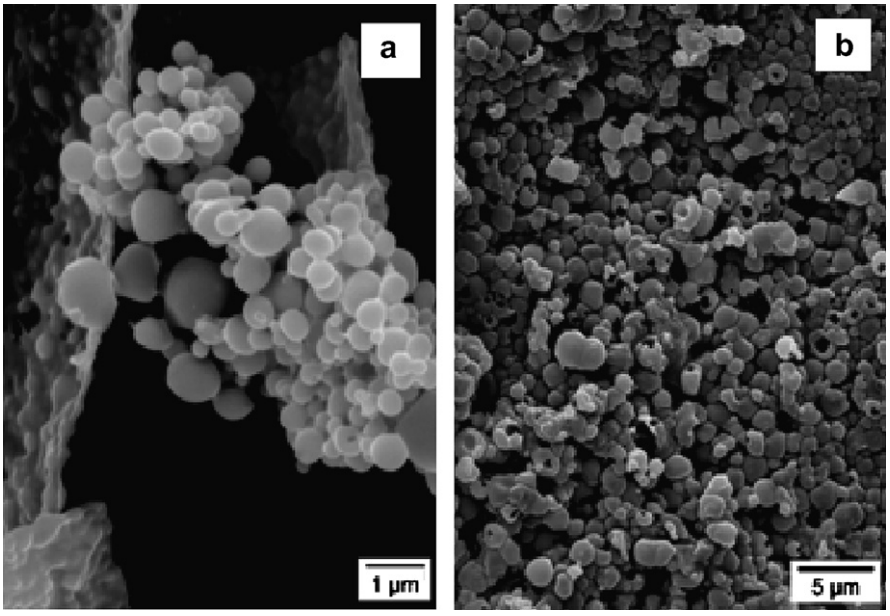

Fig. 13. (a) SEM micrograph of rhenium-loaded nanoparticles irradiated at 1×10^{11} n/cm^2/s for 30 min (bar = 1 μm). (b) SEM micrograph of $Re_2(CO)_{10}$ loaded nanoparticles irradiated at 1.45×10^{13} n/cm^2/s for 1 h (bar = 1 μm).

tron flux of 1.45×10^{13} n/cm^2/s during 1 h. The large thermal neutron cross-section of ^{186}Re and ^{188}Re enabled high specific activities to be achieved in short neutron activation times without any detected radioactive contaminants. The obtained radioactivities were measured at the end of neutron irradiation. At a rhenium content around 23% w/w (batch D), the obtained radioactivity was 1.71×10^{05} μCi (^{186}Re)/g Np and 6.98×10^{05} μCi (^{188}Re)/g Np which equals 8.69×10^{05} μCi (^{total}Re)/g Np or 32.5 GBq (^{total}Re)/g Np. A similar specific activity value has been also mentioned by Hafeli et al. [12]. The authors prepared 30% w/w rhenium metal-loaded PLLA microparticles (median size = 22 μm) and activated them by a relatively similar neutron flux of 1.5×10^{13} n/cm^2/s during 1 h to obtain 31.8 GBq (^{total}Re)/g microparticles. Furthermore, the group of Nijsen et al. [40] reported the elaboration of holmium acetylacetonate loaded PLLA microparticles (20–50 μm) at a 17% holmium loading. In their paper, Nijsen et al. bombarded their microparticles with a relatively 3 times higher neutron flux of 5×10^{13} n/cm^2/s during 1 h and obtained a specific activity of 50 GBq (^{166}Ho)/g microparticles which seems to be not far also from ours.

As it has been highlighted above, our overall objective was to prepare highly rhenium-loaded nanoparticles yielding high radioactivities after neutron activation for an intra-tumoral radionuclide therapy. Thereafter, we have applied a relatively similar predictive analysis to that of Conzone et al. [63] concerning the potential utilisation of our nanoparticles for such potential application. If we prepare a suspension of 100 μl containing 50 mg of our nanoparticles loaded with 23% w/w rhenium element, this will yield a suitable sufficient radioactivity for intra-tumoral radionuclide therapy. Indeed, this can be explained as follows; the activation of such nanoparticles amount at the above-mentioned conditions would yield the production of 1020 MBq ^{188}Re and 176 MBq ^{186}Re. Assuming a necessary period of one day to ship the radiopharmaceutical to the hospital, thus one day later, the remaining radioactivity at the time of intra-tumoral administration would be 383 MBq ^{188}Re and 146 MBq ^{186}Re (Eq. (2)). According to O'Donoghue's data [64], the necessary radioactivity to attain one gram weighted tumor curability of 90% is 4.97 MBq of ^{186}Re or 6.03 MBq of ^{188}Re. Now, assuming that the nanoparticles are homogeneously distributed throughout the tumor mass, and that the same cure probability of 90% is required, then a spherical tumor of around 40 g or 4.2 cm diameter could be treated with this radioactivity. Furthermore, as it has been explained above, at a day elapsed time after activation, the mixture of ^{188}Re and ^{186}Re would be at a ratio of about 3 to 1. Indeed, taking into account this high initial percentage of ^{188}Re, with a relatively short half-life of 17 h, this should improve the radiobiological efficacy as the radiation is given at a high initial dose rate. Many tumor cell lines have been shown to be much more resistant to radiation at lower dose rates as that allows for DNA repair and repopulation [65].

Finally, to calculate the predicted absorbed radiation dose (Gy) in a brain tumor model, the nodule module in Mirdose 3.1 software (Oak Ridge Institute for Science and Education, USA) was used. Theoretically, the tumor dose after a complete decay of the two isotopes ^{186}Re and ^{188}Re can be calculated from the following equation.

$$D = A^{186}.S^{186} + A^{188}.S^{188} = \mathrm{M}(A_s^x/\lambda_x)_{186}.S^{186} + \mathrm{M}(A_s^x/\lambda_x)_{188}.S^{188} \quad (5)$$

where D is the absorbed dose (Gy), A is the intra-tumoral cumulated radioactivity (GBq s), M is the mass of injected nanoparticles (g), A_s^x is the initial radioactivity (GBq/g Np), λ_x is the decay constant of the respective isotope (s^{-1}) and S is the S-value (mean tissue absorbed dose per unit of cumulative activity, Gy GBq^{-1} s^{-1}).

Using Mirdose 3.1 software allows us to use the tabulated values of S-values which largely facilitate calculations. Considering now a brain tumor of 40 g (4.2 cm diameter) and a 50 mg nanoparticles remained radioactivity of 383 MBq ^{188}Re and 146 MBq ^{186}Re, after a one day cooling period as mentioned above, by using this software, the calculated tumor absorbed dose after a nanoparticles intra-tumoral residence period of 2 weeks was found to be 40 Gy (from ^{188}Re) and 7 Gy (from ^{186}Re). That means that the total absorbed dose into this brain tumor model is around 47 Gy; being achieved from a sole injection of 50 mg activated nanoparticles, which is a comparable value to that mentioned by Conzone et al. [63], without forgetting the difference between the S-values of the two different supposed tissues in the two studies (the brain and the liver). The later authors estimated the obtained absorbed dose into a hepatic tumor to be up to 100 Gy after the injection of 50 mg of 13% rhenium-loaded glass microparticles. However, in the work of Conzone et al. [63], the specific radioactivity of glass microparticles was higher as the microparticles were bombarded at a largely stronger neutron flux of up to 8×10^{13} n/cm^2/s (about 5 times stronger than ours) and during 8 times longer time (8.2 h in their study).

Conclusion

The overall objective of this study was to develop a well-characterized method for a reproducible preparation of rhenium-loaded PLLA based nanoparticles. Dirhenium decacarbonyl [$Re_2(CO)_{10}$] has been encapsulated in poly(L-lactic acid) nanoparticles using an oil-in-water emulsion–solvent evaporation method. A 3^3 factorial design has been performed to investigate the influence of different proceeding and formulation parameters on both the nanoparticles size and the rhenium encapsulation efficacy. The nanoparticles size ranged between 330 and 1500 nm and the maximum rhenium element loading was 24% w/w. DSC assays showed that the $Re_2(CO)_{10}$ was encapsulated in its crystalline initial state. Other experiments including FT-IR and NMR did not show interac-

tions between PLLA and $Re_2(CO)_{10}$. Thereafter, these nanoparticles have been bombarded with a neutron flux of 1.45×10^{13} n/cm^2/s during 1 h achieving a specific activity of about 32.5 GBq per gram of nanoparticles. Preliminary estimations via Mirdose 3.1 software have shown that a sole injection of 50 mg of activated nanoparticles into a brain tumor would deliver a tumor absorbed dose as high as 47 Gy. In conclusion, we would think that these dirhenium decacarbonyl-loaded nanoparticles can be a novel promising tool for a radionuclide intra-tumoral therapy.

Acknowledgement

The authors would like to thanks Dr. Urs Hafeli (University of British Columbia, Canada) for supplying the Mirdose 3.1 software. The authors are also grateful to Mr. Xavier Jauravd for EDS analysis.

References

[1] S.S. Feng, Nanoparticles of biodegradable polymers for new-concept chemotherapy, Expert Rev. Med. Devices 1 (2004) 115–125.
[2] I.M. Ariel, G.T. Pack, Treatment of inoperable cancer of the liver by intra-arterial radioactive isotopes and chemotherapy, Cancer 20 (1967) 793–804.
[3] M.P. Osborne, J.H. Payne, V.J. Richardson, V.R. McCready, B.E. Ryman, The preoperative detection of axillary lymph node metastases in breast cancer by isotope imaging, Brit. J. Surg. 70 (1983) 141–144.
[4] K.L. Meehan, M.D. Sadar, Quantitative profiling of LNCaP prostate cancer cells using isotope-coded affinity tags and mass spectrometry, Protiomecs 4 (2004) 1116–1134.
[5] D.M. Kaylie, K.R. Stevens, M.Y. Kang, J.I. Cohen, M.K. Wax, P.E. Andersen, External beam radiation followed by planned neck dissection and brachytherapy for base of tongue squamous cell carcinoma, Laryngoscope 110 (2000) 1633–1636.
[6] K. Kostarelos, D. Emfietzoglou, Tissue dosimetry of liposome-radionuclide complexes for internal radiotherapy: toward liposome-targeted therapeutic radiopharmaceuticals, Anticancer Res. 20 (2000) 3339–3345.
[7] A. Bao, B. Goins, R. Klipper, G. Negrete, W.T. Phillips, ^{186}Re-liposome labeling using ^{186}Re-SNS/S complexes: in vitro stability, imaging, and biodistribution in rats, J. Nucl. Med. 44 (2003) 1992–1999.
[8] S.W. Zielhuis, J.H. Seppenwoolde, V.A. Mateus, C.J. Bakker, G.C. Krijger, G. Storm, B.A. Zonnenberg, A.D. van het Schip, G.A. Koning, J.F. Nijsen, Lanthanide-loaded liposomes for multimodality imaging and therapy, Cancer Biother. Radiopharm. 21 (2006) 520–527.
[9] S.W. Zielhuis, J.F. Nijsen, G.C. Krijger, A.D. van het Schip, W.E. Hennink, Holmium-loaded poly(L-lactic acid) microspheres: in vitro degradation study, Biomacromolecules 7 (2006) 2217–2223.
[10] U.O. Hafeli, G. J Pauer, J. Unnithan, R.A. Prayson, Fibrin glue system for adjuvant brachytherapy of brain tumors with (188)Re and (186)Re-labeled microspheres, Eur. J. Pharm. Biopharm. 65 (2006) 282–288.
[11] D.Y. Kim, D.S. Kwon, R. Salem, C.K. Ma, M.S. Abouljoud, Successful embolization of hepatocelluar carcinoma with yttrium-90 glass microspheres prior to liver transplantation, J. Gastrointest. Surg. 10 (2006) 413–416.
[12] Z. Chunfu, C. Jinquan, Y. Duanzhi, W. Yongxian, F. Yanlin, T. Jiaju, Preparation and radiolabeling of human serum albumin (HSA)-coated magnetite nanoparticles for magnetically targeted therapy, Appl. Radiat. Isot. 61 (2004) 1255–1259.
[13] S. Ballot, N. Noiret, F. Hindre, B. Denizot, E. Garin, H. Rajerison, J.P. Benoit, ^{99}mTc/^{188}Re-labelled lipid nanocapsules as promising radiotracers for imaging and therapy: formulation and biodistribution, Eur. J. Nucl. Med. Mol. Imaging 33 (2006) 602–607.
[14] U.O. Hafeli, W.K. Roberts, G.J. Pauer, S.K. Kraeft, R.M. Macklis, Stability of biodegradable radioactive rhenium (Re-186 and Re-188) microspheres after neutron-activation, Appl. Radiat Isot. 54 (2001) 869–879.
[15] M.J. Herba, F.F. Illescas, M.P. Thirlwell, G.J. Boos, L. Rosenthall, M. Atri, P.M. Bret, Hepatic malignancies: improved treatment with intra-arterial Y-90, Radiology 169 (1988) 311–314.
[16] J.F. Early, L. Durack, D. Williams, J.L. Vanderheyden, Consideration for imaging Re-188 and Re-186 isotopes, Clinl. Nucl. Med. 15 (1990) 911–916.
[17] E. Hiltbrand, J. Belenger, T. Binzoni, F. Buchegger, M. Costa, H. Mehier, A new method of thermoablation with hot water vapour for localized tumors, Anticancer Res. 24 (2004) 2757–2763.
[18] C. Roux, N. Rauber, E. Hiltbrand, J. Belenger, H. Khan, N. Dfouni, N. Michel, J.F. Knopf, J. Foray, H. Mehier, Experimental study on a large animal model of a new thermoablation technique, Anticancer Res. 26 (2006) 1–8.
[19] E. Hiltbrand, J. Belenger, T. Binzoni, F. Buchegger, H. Fessi, M. Costa, G. Quash, J. Foray, H. Mehier, Thérapie focalisée par micro-injections haute pression à l'aide d'un microtube implantable, ITBM-RBM 24 (2003) 136–144.
[20] H. Ozaki, T. Kinoshita, T. Kosuge, K. Shimada, J. Yamamoto, K. Tokuuye, N. Fukushima, K. Mukai, Long-term survival after multimodality treatment for resectable pancreatic cancer, Int. J. Pancreatol. 27 (2000) 217–224.
[21] F. Lefranc, N. Sadeghi, I. Camby, T. Metens, O. Dewitte, R. Kiss, Present and potential future issues in glioblastoma treatment, Expert Rev. Anticancer Ther. 6 (2006) 719–732.
[22] S. Buono, N. Burgio, M. Hamoudeh, H. Fessi, E. Hiltbrand, L. Maciocco, S. Mehier-Humbert, Brachytherapy: state of the art and possible improvements, Curr. Med. Chem. Anti-Cancer Drug 7(4) (2007) in press.
[23] M. Hamoudeh, A. Al Faraj, E. Canet-Soulas, F. Bessueille, D. Léonard, H. Fessi, Elaboration of PLLA-based superparamagnetic nanoparticles: characterization, magnetic behaviour study and in vitro relaxivity evaluation, Int. J. Pharm., doi:10.1016/ijpharm.2007.01.023.
[24] S.W. Zielhuis, J.F. Nijsen, R. Figueiredo, B. Feddes, A.M. Vredenberg, A.D. Van het Schip, W.E. Hennink, Surface characteristics of holmium-loaded poly(L-lactic acid) microspheres, Biomaterials 26 (2005) 925–932.
[25] N.A. Armstrong, K.C. James, Understanding Experimental Design and Interpretation in Pharmaceutics, Ellis Horwood, Chichester, UK, 1990.
[26] N. Erden, N. Celebi, Factors influencing release of salbutamol sulphate from poly(lactide-co-glycolide) microspheres prepared by water-in-oil-in-water emulsion technique, Int. J. Pharm. 137 (1996) 57–66.
[27] J. Vandervoort, A. Ludwig, Biocompatible stabilisers in the preparation of PLGA nanoparticles: a factorial design study, Int. J. Pharm. 238 (2002) 77–92.
[28] S. Wold, A. Ruhe, H. Wold, W.J. Dunn, The collinearity problem in linear regression. The partial least squares (PLS) approach to generalized inverses, SIAM J. Sci. Stat. Comp. 4 (1984) 735–743.
[29] H.Y. Kwon, J.Y. Lee, S.W. Choi, Y. Jang, J.H. Kim, Preparation of PLGA nanoparticles containing estrogen by emulsification-diffusion method, Colloid Surf. A 182 (2001) 123–130.
[30] P.B. O'Donnell, J.W. McGinity, Preparation of microspheres by the solvent evaporation technique, Adv. Drug Deliv. Rev. 28 (1997) 25–42.
[31] J.Y. Zhang, Z.G. Shen, J. Zhong, T.T. Hu, J.F. Chen, Z.Q. Ma, Y. Jimmy, Preparation of amorphous cefuroxime axetil nanoparticles by controlled nanoprecipitation method without surfactants, Int. J. Pharm. 323 (2006) 153–160.

[32] M. Hamoudeh, H. Fessi, Preparation, characterization and surface study of poly-epsilon caprolactone magnetic microparticles, J. Colloid Interf. Sci. 300 (2006) 584–590.
[33] D. Quintanar-Guerrero, H. Fessi, E. Allémann, E. Doelker, Influence of stabilizing agents and preparatives variables on the formation of poly(d,l-lactic acid) nanoparticles by an emulsification-diffusion technique, Int. J. Pharm. 143 (1996) 133–141.
[34] H. Murakami, M. Kobayashi, H. Takeuchi, Y. Kawashima, Preparation of poly(DL-lactide-co-glycolide) nanoparticles by modified spontaneous emulsification solvent diffusion method, Int. J. Pharm. 187 (1999) 143–152.
[35] M. Chorny, I. Fishbein, H.D. Danenberg, G. Golomb, Lipophilic drug loaded nanospheres prepared by nanoprecipitation: effect of formulating variables on size, drug recovery and release kinetics, J. Control. Release 83 (2002) 389–400.
[36] Y.Y. Yang, T.S. Chung, N.P. Ng, Morphology, drug distribution, and in vitro release profiles of biodegradable polymeric microspheres containing protein fabricated by double-emulsion solvent extraction/evaporation method, Biomaterials 22 (2001) 231–241.
[37] M.D. Bhavsar, S.B. Tiwari, M.M. Amiji, Formulation optimization for the nanoparticles-in-microsphere hybrid oral delivery system using factorial design, J. Control. Release 110 (2006) 422–430.
[38] P. Eun Kyoung, L. Sang Bong, L. Young Moo, Preparation and characterization of methoxy poly(ethylene glycol)/poly(ε-caprolactone) amphiphilic block copolymeric nanospheres for tumor-specific folate-mediated targeting of anticancer drugs, Biomaterials 26 (2005) 1053–1061.
[39] S.K. Sahoo, J. Panyam, S. Prabha, V. Labhasetwar, Residual polyvinyl alcohol associated with poly (D,L-lactide-co-glycolide) nanoparticles affects their physical properties and cellular uptake, J. Control. Release 82 (2002) 105–114.
[40] J.F. Nijsen, B.A. Zonnenberg, J.R. Woittiez, D.W. Rook, I.A. Swildens-van Woudenberg, P.P. van Rijk P, A.D. van het Schip, Holmium-166 poly lactic acid microspheres applicable for intra-arterial radionuclide therapy of hepatic malignancies: effects of preparation and neutron activation techniques, Eur. J. Nucl. Med. 26 (1999) 699–704.
[41] T. Gorner, R. Gref, D. Michenot, F. Sommer, M.N. Tran, E. Dellacherie, Lidocaine-loaded biodegradable nanospheres. I. Optimization of the drug incorporation into the polymer matrix, J. Control. Release 57 (1999) 259–268.
[42] P.C. Chen, Y.J. Park, L.C. Chang, D.S. Kohane, R.H. Bartlett, R. Langer, V.C. Yang, Injectable microparticle-gel system for prolonged and localized lidocaine release. I. In vitro characterization, J. Biomed. Mater. Res. A 70 (2004) 412–419.
[43] Z. El Bahri, J.L. Taverdet, Preparation and optimization of 2,4-D loaded cellulose derivatives microspheres by solvent evaporation technique, J. Appl. Polym. Sci. 103 (2006) 2742–2751.
[44] Z. El Bahri, J.L. Taverdet, Elaboration and characterization of microparticles loaded by pesticide model, Powder Technol. 172 (2007) 30–40.
[45] S.S. Feng, G. Huang, Effects of emulsifiers on the controlled release of paclitaxel (Taxol®) from nanospheres of biodegradable polymers, J. Control. Release 71 (2001) 53–69.
[46] A. Carrio, G. Schwach, J. Coudane, M. Vert, Preparation and degradation of surfactant-free PLAGA microspheres, J. Control. Release 37 (1991) 113–121.
[47] F. Boury, T.Z. Ivanova, I. Panaiotov, J.E. Proust, A. Bois, J. Richou, Dynamic properties of poly(DL-lactide) and polyvinyl alcohol monolayers at the air/water and dichloromethane/water interfaces, J. Colloid Interf. Sci. 169 (1995) 380–392.
[48] M.F. Zambaux, F. Bonneaux, R. Gref, P. Maincent, E. Dellacherie, M.J. Alonso, P. Labrude, C. Vigneron, Influence of experimental parameters on the characteristics of poly(lactic acid) nanoparticles prepared by a double emulsion method, J. Control. Release 50 (1998) 31–40.
[49] H. Xu, C. Teng, M. Yu, Improvements of thermal property and crystallization behavior of PLLA based multiblock copolymer by forming stereocomplex with PDLA oligomer, Polymer 47 (2006) 3922–3928.
[50] Y. Ikada, K. Jamshidi, H. o Tsuji, S.H. Hyon, Stereocomplex formation between enantiomeric poly(lactides), Macromolecules 20 (1987) 904–906.
[51] P.T. Tayade, R.D. Kale, Encapsulation of water-insoluble drug by a cross-linking technique: effect of process and formulation variables on encapsulation efficiency, particle size, and in vitro dissolution rate, AAPS PharmSci. 6 (2004) (article 12).
[52] J. Lee, T. Isobe, M. Senna, Preparation of ultrafine Fe_3O_4 particles by precipitation in the presence of PVA at high pH, J. Colloid Interface Sci. 177 (1996) 490–494.
[53] N.T. Paragkumar, D. Edith, J.L. Six, Surface characteristics of PLLA and PLGA films, Appl. Surf. Sci. 253 (2006) 2758–2764.
[54] S. Firth, P.M. Hodges, M. Poliakoff, J.J. Turner, Comparative matrix isolation and time-resolved infrared studies on the photochemistry of $MnRe(CO)_{10}$ and $Re_2(CO)_{10}$ evidence for CO-bridged $MnRe(CO)_9$, Inorg. Chem. 25 (1986) 4608–4610.
[55] C. Dubernet, Thermoanalysis of microspheres, Thermochim. Acta 248 (1995) 259–269.
[56] H. Zhang, S. Gao, Temozolomide/PLGA microparticles and antitumor activity against Glioma C6 cancer cells in vitro, Int. J. Pharm. 329 (2007) 122–128.
[57] R. Bodmeier, H. Chen, Preparation and characterization of microspheres containing the anti-inflammatory agents, indomethacin, ibuprofen, and ketoprofen, J. Control. Release 10 (1989) 167–175.
[58] S. Sosnowski, Poly(L-lactide) microspheres with controlled crystallinity, Polymer 42 (2000) 637–643.
[59] M.B. Sintzel, K. Schwach-Abdellaoui, K. Mäder, R. Stösser, J. Heller, C. Tabatabay, R. Gurny, Influence of irradiation sterilization on a semi-solid poly(*ortho* ester), Drug Develop. Ind. Pharm. 175 (1989) 165–176.
[60] P. Lemoine, M. Gross, J. Bousquet, M. Letoffe, M. Diot, Thermodynamic results on a solid-phase transition in dimanganese and dirhenium decacarbonyls, J. Chem. Thermodyn. 7 (1975) 913–917.
[61] P. Lemoine, M. Gross, Decomposition thermique du dimanganese Decacarbonyle et du dirhenium decacarbonyle, J. Therm. Anal. Calorim. 6 (1974) 159–173.
[62] R.J. Mumper, M. Jay, Poly(L-lactic acid) microspheres containing neutron-activatable holmium-165: a study of the physical characteristics of microspheres before and after irradiation in a nuclear reactor, Pharm. Res. 9 (1992) 149–154.
[63] S.D. Conzone, U.O. Hafeli, D.E. Day, G.J. Ehrhardt, Preparation and properties of radioactive rhenium glass microspheres intended for in vivo radioembolization therapy, J. Biomed. Mater. Res. 42 (1998) 617–625.
[64] J.A. O'Donoghue, M. Bardies, T.E. Wheldon, Relationships between tumor size and curability for uniformly targeted therapy with beta-emitting radionuclides, J. Nucl. Med. 36 (1995) 1902–1909.
[65] J. Carlsson, E. Hakansson, V. Eriksson, J. Grawe, K. Wester, E. Grusell, A. Montelius, H. Lundqvist, Early effects of low dose-rate radiation on cultured tumor cells, Cancer Biother. Radio. 18 (2003) 663–670.